Heat and mass transfer coefficients of falling-film absorption on a partially wetted horizontal tube

Heat and mass transfer coefficients of falling-film absorption on a partially wetted horizontal tube

Niccolò Giannetti[1*], Andrea Rocchetti[2], Seiichi Yamaguchi[1], Kiyoshi Saito[1]

[1] Department of Applied Mechanics and Aerospace Engineering, Waseda University
3-4-1 Okubo, Shinjuku-ku, Tokyo 169-8555, Japan
[2] Department of Industrial Engineering of Florence, University of Florence
Via Santa Marta 3, Firenze, 50139, Italy
[*] Corresponding author: niccolo@aoni.waseda.jp

Abstract- Detailed, reliable, and time-saving methods to predict the transfer characteristics of horizontal-tube falling-film absorbers are critical to control system operability, such that it is closer to its technical limitations, and to optimise increasingly complex configurations. In this context, analytical approaches continue to hold their fundamental importance. This study presents an analytical solution of the governing transport equations of film absorption around a partially wetted tube. A film stability criterion and a wettability model extend the validity range of the resulting solution and increase its accuracy. Temperature and mass fraction fields are analytically expressed as functions of Prandtl, Schmidt, and Reynolds numbers as well as tube dimensionless diameter and wetting ratio of the exchange surface. Inlet conditions are arbitrary. The Lewis number and a dimensionless heat of absorption affect the characteristic equation and the corresponding eigenvalues. Consequently, local and average transfer coefficients are estimated and discussed with reference to the main geometrical and operative parameters. Finally, a first comparison with the numerical solution of the problem and experimental data from previous literature is presented to support the simplifying assumptions, which are introduced and as a first model validation.

Nomenclature

A, B	Eigenfunction coefficients
a, b	Power series coefficients
c_p	Isobaric specific heat, $J\cdot kg^{-1}K^{-1}$
D	Mass diffusivity, $m^{2}\cdot s^{-1}$
d	Diameter, m
E, H	Single variable exponential functions
F, G	Eigenfunctions
g	Gravity, $m\cdot s^{-2}$
h	Specific enthalpy, $kJ\cdot kg^{-1}$
htc	Heat transfer coefficient, $kW\cdot m^{-2}K^{-1}$
k	Thermal conductivity, $W\cdot m^{-1}K^{-1}$
l	Reference axial length, m
L_c	Characteristic length, m [$L_c=\nu^{2/3}\cdot g^{-1/3}$]
Le	Lewis number [$Le=\alpha\cdot D^{-1}$]
mtc	Mass transfer coefficient, $m\cdot s^{-1}$
Nu	Nusselt number [$Nu=htc\ L_c\cdot k^{-1}$]
P	Pressure, kPa
Pr	Prandtl number [$Pr=\nu\cdot\alpha^{-1}$]
Q	Heat flux, W
r	Outer tube radius, m
Re	Reynolds Number [$Re=4\Gamma\cdot\mu^{-1}$]
S	Area, m^2
Sc	Schmidt Number [$Sc=\mu\cdot\rho^{-1}D^{-1}$]
Sh	Sherwood Number [$Sh=mtc\ L_c\cdot D^{-1}$]
t	Tube wall thickness, m
T	Temperature, K
u	Streamwise Velocity, $m\cdot s^{-1}$
v	Normal Velocity, $m\cdot s^{-1}$
W	Transversal extension of the wet part, m
WR	Wetting Ratio
x	Local tangential position, m
y	Local normal position, m

Greek symbols

α	Thermal diffusivity, $m^{2}\cdot s^{-1}$
β	Contact angle
ε	Dimensionless tangential position
γ	Dimensionless LiBr mass fraction distribution
η	Dimensionless normal position
Λ	Normalised heat of absorption [$\Lambda=h_{abs}(\omega_e-\omega_{in})\cdot(T_e-T_{in})^{-1}\ \omega_e^{-1}c_p^{-1}$]
λ,ϕ	Eigenvalues
θ	Dimensionless temperature distribution
Γ	Mass flow rate per unit length, $kg\cdot s^{-1}m^{-1}$
δ	Film thickness, m
μ	Dynamic viscosity, $Pa\cdot s$
ρ	Density, $kg\cdot m^{-3}$
ω	LiBr mass fraction

Subscripts

0	Film breaking condition
abs	Absorption
av	Average
b	Bulk value
c	Cooling water side
e	Equilibrium
g	Global
i	Power series index
if	Interface
in	Inlet
max	Maximum
n, m	Eigenvalue/Eigenfunction indexes
o	Outlet
sat	Phases equilibrium
T	Temperature
v	Vapour
W	Wall

		*	Dimensionless

Superscripts

1. Introduction

It is not possible to consider heat transfer and mass transfer separately in several technical circumstances and physical processes. Absorption systems, such as chillers, heat amplifiers, and heat transformers, belong to the aforementioned category and represent an opportunity for clean and efficient energy conversion systems (1). The main advantages of these systems include low-grade heat as the main energy source, higher reliability, and environmentally friendly refrigerants. This is accompanied by the possibility of realising the refrigerant pressure jump in a liquid phase. Accordingly, the compressor of a conventional system is substituted with a set of components, such as a solution pump, a generator, an absorber, and a solution heat exchanger, termed as a “thermal compressor”. As a downside, this requires a significantly larger exchange surface. In addition, extant studies indicated that the highest amount of irreversibility occurs in an absorber (2) and that global capacity and first law efficiency are limited by the amount of refrigerant that is absorbed in this component (3–4). Therefore, the intensification of the absorption process and proper design of an absorber are the critical factors that should be addressed. Conversely, the recent technical development of absorption chillers, heat pumps, and heat transformers corresponds to increasingly complex plant configurations (5–6), and specifically constitutes a step forward with respect to the theoretical background required for an accurate performance prediction, optimisation, and control. In general, the systems design approach continues to rely on empirical rules, heuristic correlations, or trial and error procedures on a global and component scale. The correlations rely on large sets of data, in which each set depends on experimental equipment as well as the

specific boundary conditions of these measurements. Furthermore, devices that are designed to achieve high performance under nominal conditions may not exhibit a sufficient performance over most of the actual operative range. Similarly, in practice, conditions are transient and change continuously, because they are affected by interrelations with the external environment. Consequently, instantaneous conditions significantly differ from the design point. The construction of reliable and widely applicable theoretical models enables the design, optimisation, and definition of an effective control method without depending on trial and error procedures or empirical rules.

More specifically, horizontal-tube falling-film absorbers can realise high heat and mass transfer rates with compact size and negligible pressure losses. Nevertheless, prior experimental studies on falling film absorption (7–12) report a limited amount of results with high uncertainties and within a relatively narrow range of operative conditions.

Reference (13) numerically discusses a model for film absorption and desorption of a laminar liquid film with constant thickness that flows over a vertical isothermal plate. A similar model was applied by (14) to a horizontal tube heat exchanger. References (15–18) introduce the effects of thickness and velocity distributions around a tube surface via numerical analyses. Finally, references (19–25) use the Volume of Fluid technique to examine and extract detailed descriptions of the wavy film dynamics, inter-tube droplets formation, detachment, and impact. Numerical analysis and computational fluid dynamics (CFD) are powerful tools that could be very precise when the problem is properly formulated. However, it is necessary to adequately consider the time required to reach an accurate solution and the fact that its validity is restricted to the specific case and the selected operative condition. Generalisable design guidelines are not directly provided by specific results as well as heuristic methods. Given this viewpoint, analytical approaches continue to maintain their fundamental importance to

capture the physics of the problem and generalise the validity of the solution. The main limitations of extant analytical models include the geometry of the solid surface, assumptions of complete wetting, equilibrium of an inlet solution with the refrigerant vapour, uniform velocity profile, and film thickness (26–29). Reference (28) indicated that uniform velocity profile and film thickness are responsible for approximately 20% deviations in the heat and mass transfer coefficients, and they under-predict approximately 40% of the distance required for the development of the thermal boundary layer. Therefore, this study successfully achieves an accurate and widely applicable analytical solution of the governing equations of falling film absorption over a horizontal tube including the effects of thickness variations, incomplete wetting, and the corresponding reduction in transfer interfaces.

2. Physical model

The present analysis focuses on an absorptive liquid film flowing over a vertical row of horizontal smooth tubes. Droplet impact and hydrodynamic boundary layer development (19–25, 30) are not discussed herein. Figure 1 schematically illustrates the system under consideration. A single tube at uniform wall-temperature, T_w, is considered. A thin film of LiBr–H_2O solution impinges at the top (x=0) and flows viscously down the tube due to gravity as a laminar incompressible liquid. Additionally, absorption can occur at the free-interface of the film based on the thermo-physical relation between the solution and the vapour. The enthalpy of vapour condensation that is released in the lithium-bromide/water mixture is rejected to the cooling water flowing inside the tube. Following the development of the thermal boundary layer, the temperature gradient related to the cooling process at the wall also influences the temperature at the interface, and this in turn establishes the equilibrium mass

fraction at the vapour pressure within the heat exchanger and consequently controls mass transfer.

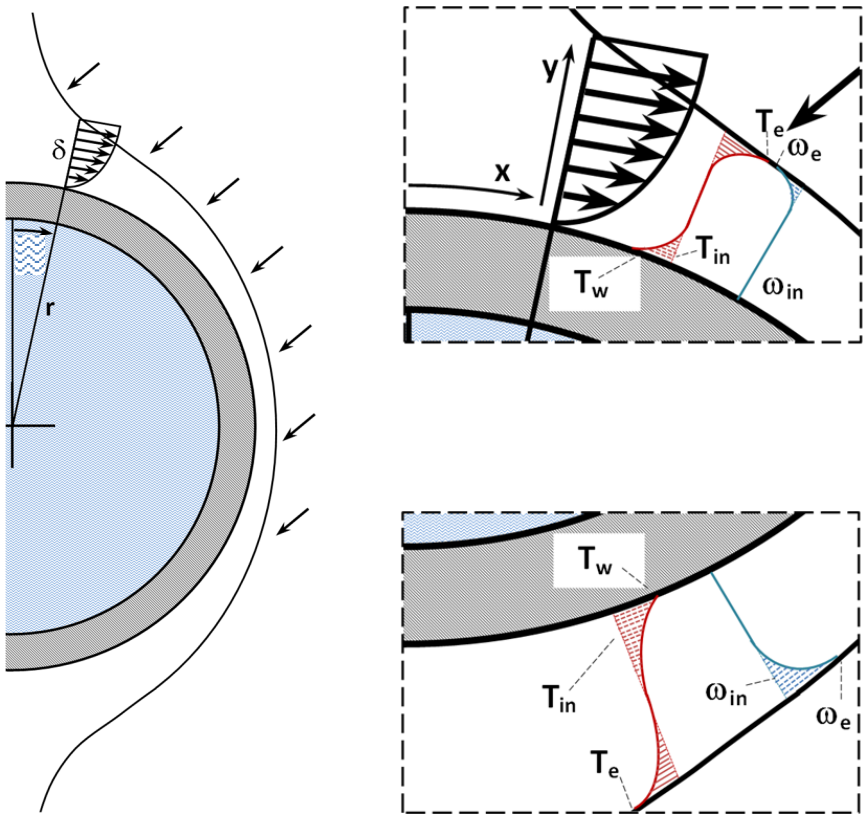

Figure 1. Local coordinate system

In order to reach a closed analytical solution of the governing transport equations, heat and mass transfer processes are considered under the following main assumptions:

- The zone of impingement is assumed as a small fraction of the total periphery, and it is assumed that the thermal boundary layer starts its growth from the upper stagnation point ($x \approx 0$);
- It is assumed that both the tube circumference and length are large when compared to the film thickness and that the disturbances at the edges of the system can be neglected;
- The flow is laminar;
- Neither interfacial shear forces with the vapour nor interfacial waves exist;

- Thermodynamic equilibrium occurs at the film inlet-interface with the vapour at the heat exchanger pressure, and thus mass transfer occurs without any resistance;
- Thermo-physical solution properties are similar to those of an ideal mixture and remain constant along the film thickness and around the tube. As a corollary, natural and Marangoni convection are not considered;
- Heat transfer to the vapour environment is neglected;
- The variation of the mass flowrate due to the absorbed vapour is negligible;
- According to the thin film approximation introduced by (27), body fitted coordinates (x along the tube surface and y normal to it at any point) are used because the film thickness is low when compared to the tube diameter.

A curvilinear coordinate transformation is adopted to map the flow domain of the physical space to a simple rectangular domain (16). The dimensionless variables considered in the circumferential and radial directions correspond to $\varepsilon=x/\pi r$ and $\eta=y/\delta$, respectively. Tangential (eq. 1) and normal (eq. 2) velocity components based on the Nusselt integral solution of the boundary layer momentum and continuity equations with constant properties form (see, for instance, references 13-18) are employed under the assumption that the momentum transfer of the fluid is dominated by viscous forces in the absence of inertia and pressure forces.

$$u = \frac{\rho g \delta^2}{2\mu} \sin \pi\varepsilon \left(2\eta - \eta^2\right) \tag{1}$$

$$v = -\frac{\rho g \delta^2 \eta^2}{2\mu r} \left[\frac{1}{\pi} \frac{d\delta}{dx} \sin \pi\varepsilon + \delta \left(1 - \frac{\eta}{3}\right) \cos \pi\varepsilon \right] \tag{2}$$

Accordingly, once the film mass flowrate per unit length of the tube is known, the corresponding film thickness is given by eq. 3.

$$\delta = \left(\frac{3\mu\Gamma}{\rho^2 g \sin\pi\varepsilon} \right)^{1/3} \quad (3)$$

A small thermal resistance is associated with a thinner film at low specific mass flowrates, and thus moving the operability of falling film absorbers to a low Reynolds number is attractive in increasing the performance of absorption systems and reducing their overall size. However, it is necessary to consider the reduction in the contact area due to partial wetting as a critical related issue. In these operative conditions, specifically at a low film Reynolds number ($Re=4\Gamma/\mu$) and while employing liquids with high surface tension (i.e., low Weber numbers), it is not possible to consider the assumptions of a film with uniform thickness and complete wetting of the transfer surface as even approximately rigorous. This leads to an unacceptable inaccuracy of simulation results (i.e., the obtained trend of the predicted heat transfer coefficient itself disagrees with measurements (31)). Furthermore, it is recognised that partial wetting occurs even at typical operative conditions. Among the previously proposed models, the effect of the amount of wetted surface is not assessed or is merely assumed as a fixed value imposed on the calculation (15, 32) albeit with a few exceptions (9, 33–35). Moreover, related experimental data and visual descriptions by digital image processing are also extremely limited in terms of the number of studies that report the same as well as in the range of conditions that is covered (36–39). Nevertheless, the role of wettability is recognised as a dominant factor in determining the efficiency of the absorption process. Therefore, both a criterion of stability of the uniform film to identify the minimum flow rate to ensure a complete wetting of the surface and a method to estimate the wetted area after the film breakage should be included to enhance the model capability to predict the performance of these devices.

To consider the effect of partial wetting, after the thermo-physical properties of the solution are given, the extension of the range affected by the phenomenon is identified by the critical condition for a uniform film in terms of minimum wetting rate Γ_0 that corresponds to a critical Reynolds number Re_0. The latter can be experimentally measured (37-41) or analytically estimated for a surface with generic inclination (42-43) once the characteristic contact angle that is representative of the affinity of the solid-liquid interaction is known. Among the various available methods (44-47), the principle of minimising the energy contained in a given stream wise length of the falling film is hereby used to assess the stability of the uniform configuration (eq. 4) and to provide an estimate (eq. 5) of the rivulet wetting ability (42-43) given the assumption of a rivulet cross-section geometry. The value of the dimensionless group $(Re_0 \cdot We_0^3)^{1/15}$ in (43) is directly proportional to the dimensionless critical thickness δ_0^* that is defined in (42) (eq. 4). Therefore, equation 4 represents the flow regime transition between a uniform film and a rivulet flow configuration with circular cross-section shape and contact angle β, which partially wets the solid surface. This is obtained from the condition of equivalent kinetic plus surface tension energy, and flowrate of the two regimes, when the stable condition of the rivulet is identified through the principle of minimum energy.

$$\delta_0^{*5} + (1-\cos\beta) - G(\beta)\,\delta_0^{*3} = 0 \qquad , \qquad \delta_0^{*} = \left(\frac{\rho^3 g^2}{15\mu^2\sigma}\right)^{1/5} \delta_0 \tag{4}$$

Equation 5 corresponds to the minimisation of the energy contents of a given stream-wise length of the rivulet, with respect to the geometrical parameter that defines its wetting ability WR (the ratio of the base of the rivulet w to the total axial length l taken as a reference).

$$WR = \left\{ \frac{1}{15} \frac{\rho g}{\sigma} \frac{\psi(\beta)}{\sin\beta} \left[\frac{\beta}{\sin\beta} - \cos\beta \right]^{-1} \right\}^{3/5} \frac{\sin\beta}{\gamma(\beta)} \mathrm{Re} \quad (5)$$

where $G(\beta)$, $\psi(\beta)$, and $\gamma(\beta)$ denote geometrical functions of the contact angle β between the liquid-gas interface of the rivulet (further details are given in reference 43). When *WR* is used to estimate the wetting ability of the film along the absorber tube, its value corresponds to the ratio of the wetted portion *w* to the tube unit length *l* (Figure 2).

For lower solution flowrates, methods based on the principle of minimum energy (eq. 5) as well as experiments (37–41, 43) are in agreement with a linearised wettability model (eq. 6) relative to the film Reynolds number, which gives zero wetting when Reynolds number is zero, and complete wetting at $Re=Re_0$.

$$WR = \frac{\mathrm{Re}}{\mathrm{Re}_0} \quad (6)$$

Therefore, δ_0^* can be evaluated from eq. 4, once the value of the characteristic contact angle of the liquid-solid pair is known. Afterwards, using the Nusselt velocity profile for a vertical falling film, the film thickness can be directly related to the film Reynolds number ($Re=4\Gamma/\mu$) and the critical Reynolds number at which the film breaking occurs Re_0 is calculated as in eq. 7.

$$\mathrm{Re}_0 = \left(\frac{3^5 g \mu^4}{4^5 15^3 \rho \sigma^3} \right)^{-1/5} \delta_0^{*3} \quad (7)$$

The approach aims at estimating the wetted exchange area on an average basis while not targeting a local description of the complex film hydrodynamics. Furthermore, a closed solution requires considering *WR* as an independent function of the angular position on the tube surface. Accordingly, the film thickness distribution (eq. 9) is adjusted to assure the consistency

between uniform and partial wetting configurations (eq. 8) by using a modified form of the Nusselt equation (as in (32)).

$$\frac{\Gamma}{2WR} = \int_0^{\delta} \rho u(y)dy = \frac{1}{3}\frac{\rho^2 g \sin\beta}{\mu}\delta^3 \tag{8}$$

$$\delta = \left(\frac{3\mu\Gamma}{WR\rho^2 g \sin\pi\varepsilon}\right)^{1/3} \tag{9}$$

To the authors' knowledge, a direct validation of eq. 9 has not been achieved in previous literature and further research efforts in this regard are needed.

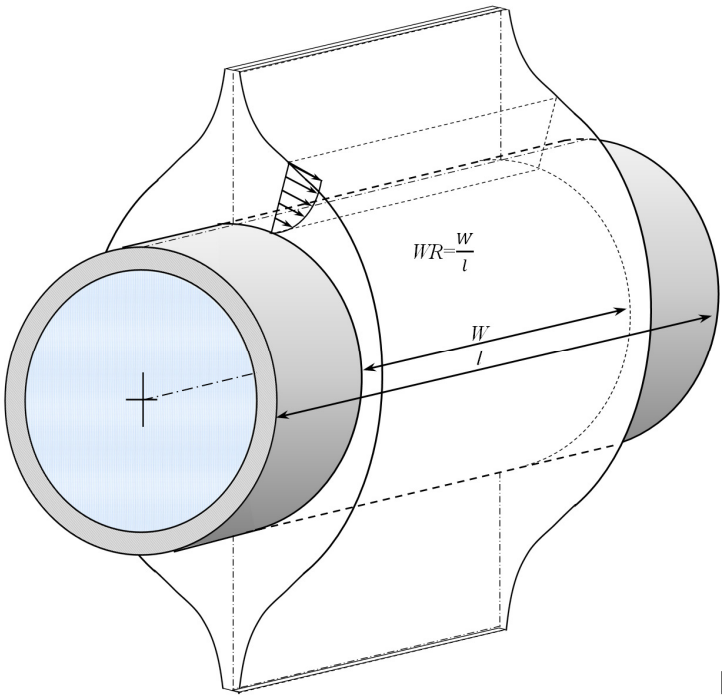

Figure 2. A physical model of film partial wetting

Heat and mass transfer characteristics of the system under analysis are studied with reference to eq.s 10 and 11. This two-dimensional form of the energy and species transport equations is written for a steady flow with constant properties without internal heat generation and viscous dissipation and neglecting

diffusion terms in the flowing direction (see, for instance, 15-16, 27).

$$\frac{\partial T}{\partial \varepsilon} = \frac{\pi r \alpha}{u\delta^2}\frac{\partial^2 T}{\partial \eta^2} + \left(\frac{\eta}{\delta}\frac{d\delta}{d\varepsilon} - \frac{\pi r v}{u\delta}\right)\frac{\partial T}{\partial \eta} \tag{10}$$

$$\frac{\partial \omega}{\partial \varepsilon} = \frac{\pi r D}{u\delta^2}\frac{\partial^2 \omega}{\partial \eta^2} + \left(\frac{\eta}{\delta}\frac{d\delta}{d\varepsilon} - \frac{\pi r v}{u\delta}\right)\frac{\partial \omega}{\partial \eta} \tag{11}$$

Where,

$$\frac{d\delta}{d\varepsilon} = -\left(\frac{\mu\Gamma\pi^3}{9WR\rho^2 g}\right)^{1/3}\frac{1}{\sin^{1/3}\pi\varepsilon}\frac{1}{\tan\pi\varepsilon} \tag{12}$$

It is shown that eq. 13 is generally applicable for the velocity distribution expressed in eq. 1 and eq. 2.

$$\left(\frac{\eta}{\delta}\frac{d\delta}{d\varepsilon} - \frac{\pi r v}{u\delta}\right) = 0 \tag{13}$$

As a result, the simplified expression is obtained as follows:

$$\frac{\partial T}{\partial \varepsilon} = \frac{\pi r \alpha}{u\delta^2}\frac{\partial^2 T}{\partial \eta^2} \tag{14}$$

$$\frac{\partial \omega}{\partial \varepsilon} = \frac{\pi r D}{u\delta^2}\frac{\partial^2 \omega}{\partial \eta^2} \tag{15}$$

An analytical solution of the coupled set of equations is approached with the final aim of obtaining Nusselt and Sherwood number expressions in terms of the operative parameters, geometrical features, and boundary conditions.

It is advantageous for the solution of the problem to use a dimensionless form of the variables T and ω as defined by eqs. 16-17 where T_e and ω_e are defined in (28). These values are,

respectively, the equilibrium temperature of the solution at LiBr mass fraction ω_{in} and the equilibrium LiBr mass fraction of the solution at temperature T_{in}, namely, the temperature and the mass fraction reached if thermodynamic equilibrium is obtained without changes in mass fraction and temperature.

$$\theta(\varepsilon,\eta)=\frac{T(\varepsilon,\eta)-T_W}{T_e-T_W} \tag{16}$$

$$\gamma(\varepsilon,\eta)=\frac{\omega(\varepsilon,\eta)-\omega_{in}}{\omega_e-\omega_{in}} \tag{17}$$

Accordingly, T_e-T_W represents the level of sub-cooling of the wall while $\omega_e-\omega_{in}$ embodies the driving force for vapour diffusion at the inlet of the calculation domain. The dimensionless tube diameter $d^*=2\pi r/L_C$ is defined as the ratio of the tube circumference to the characteristic length L_C, which is expressed in eq. 18 as follows (17):

$$L_C=\left(\frac{\mu^2}{\rho^2 g}\right)^{1/3} \tag{18}$$

Finally, non-constant terms of eq.s 14 and 15 are developed and dimensionless variables and parameters are used to express energy and species transport equations in eq. 19 and eq. 20, respectively, in which the independent variables are separated between the sides of the equations as follows:

$$\frac{1}{d^*\sin^{1/3}\pi\varepsilon}\left(\frac{3\,\mathrm{Re}}{4WR}\right)^{4/3}\frac{\partial\theta}{\partial\varepsilon}=\frac{1}{\mathrm{Pr}\left(2\eta-\eta^2\right)}\frac{\partial^2\theta}{\partial\eta^2} \tag{19}$$

$$\frac{1}{d^*\sin^{1/3}\pi\varepsilon}\left(\frac{3\,\mathrm{Re}}{4WR}\right)^{4/3}\frac{\partial\gamma}{\partial\varepsilon}=\frac{1}{Sc\left(2\eta-\eta^2\right)}\frac{\partial^2\gamma}{\partial\eta^2} \tag{20}$$

The solution is approached with the following boundary and inlet conditions: solution temperature and mass fraction at the distributor or, by assuming that complete mixing occurs, the bulk values of the solution coming from the previous tube ($x \approx 0$ and $0<y<\delta$; $T=T_{in}$, $\theta(0,\eta)=\theta_{in}$; $\omega=\omega_{in}$, $\gamma(0,\eta)=0$), at the tube wall constant temperature and non-permeability to species are assured ($y=0$; $T=T_w$, $\theta(\varepsilon,0)=0$; $\partial\omega/\partial y=0$, $\partial\gamma/\partial\eta|_W=0$), and at the phase interface ($y=\delta$; $T=T_{sat}(\omega_{if},P)$, $\omega=\omega_{if}$) phase equilibrium is established.

$$\left.\frac{\partial\theta}{\partial\eta}\right|_{if}=\frac{\Lambda}{Le}\left.\frac{\partial\gamma}{\partial\eta}\right|_{if} \tag{21}$$

Equation 21 constitutes a rearrangement of Fick's law of diffusion and Fourier law that assures that the heat produced by absorption at the film interface is conducted through the film towards the tube surface. Where, the following expression holds and defines the normalised heat of absorption (28):

$$\Lambda=-\frac{h_{abs}\left(\omega_e-\omega_W\right)}{\omega_e c_p\left(T_e-T_W\right)} \tag{22}$$

Additionally, with respect to the vapour pressure equilibrium at the interface, a linear relation (as in (28)) between temperature and mass fraction at the film interface is employed. Accordingly, in terms of the dimensionless variables at a constant pressure, the relation expressed by eq. 23 is obtained.

$$\gamma_{if}=1-\theta_{if} \tag{23}$$

Equation 23 was found in good agreement for a wide range of operative conditions of LiBr-H_2O solution and a thermodynamic justification (although it limited to electrolytic solutions) was presented in reference (48).

3. Solution method

The dependent functions (eq.s 24–25) are assumed as a infinite series of products of a number of eigenfunctions in which each is dependent on a single variable as shown in (12) and (13).

$$\theta(\varepsilon,\eta)=\sum_{n=1}^{\infty}A_nF_n(\eta)E_n(\varepsilon) \tag{24}$$

$$\gamma(\varepsilon,\eta)=1-\sum_{n=1}^{\infty}B_nG_n(\eta)H_n(\varepsilon) \tag{25}$$

The application of this method results in four ordinary differential equations as follows:

$$\frac{1}{d^{*}\sin^{1/3}\pi\varepsilon}\left(\frac{3\,\mathrm{Re}}{4WR}\right)^{4/3}\frac{E_n'}{E_n}=\frac{1}{\mathrm{Pr}\left(2\eta-\eta^2\right)}\frac{F_n''}{F_n}=-\lambda_n^{\,2} \tag{25}$$

$$\frac{1}{d^{*}\sin^{1/3}\pi\varepsilon}\left(\frac{3\,\mathrm{Re}}{4WR}\right)^{4/3}\frac{H_n'}{H_n}=\frac{1}{Sc\left(2\eta-\eta^2\right)}\frac{G_n''}{G_n}=-\phi_n^{\,2} \tag{27}$$

The general solutions of the left members of both eq. 26 and eq. 27 are as follows:

$$E_n(\varepsilon)=e^{-\lambda_n^{\,2}d^{*}\left(\frac{4WR}{3\mathrm{Re}}\right)^{4/3}\int_0^{\varepsilon}\sin^{1/3}\pi\varepsilon\,d\varepsilon} \tag{28}$$

$$H_n(\varepsilon)=e^{-\phi_n^{\,2}d^{*}\left(\frac{4WR}{3\mathrm{Re}}\right)^{4/3}\int_0^{\varepsilon}\sin^{1/3}\pi\varepsilon\,d\varepsilon} \tag{29}$$

Where λ_n and ϕ_n denote the eigenvalues corresponding to the eigenfunctions F_n and G_n, respectively. Additionally, for the linear equilibrium condition at the interface (eq. 23) that should be satisfied for every ε, it is necessary for every n that $\lambda_n=\phi_n$. The boundary conditions at the wall require $F_n(0)=0$ and $G_n'(0)=0$, while eq. 30 and eq. 31 are obtained at the interface.

$$A_n F_n(1) = B_n G_n(1) \tag{30}$$

$$A_n F_n'(1) = -\frac{\Lambda}{Le} B_n G_n'(1) \tag{31}$$

Equation 30 and eq. 31 represent two homogeneous equations for A_n and B_n, and thus a non-null solution is reached given the condition that the determinant equals zero.

$$\frac{F_n'(1)}{F_n(1)} = -\frac{\Lambda}{Le}\frac{G_n'(1)}{G_n(1)} \tag{32}$$

Equation 32 represents the characteristic equation to determine the eigenvalues λ_n when the solution for F_n and G_n is determined. The power series solutions for the right-side members of eq. 26 and eq. 27 are expressed as follows:

$$F_n(\eta) = \sum_{i=0}^{\infty} a_{n,i}\eta^i \tag{33}$$

$$G_n(\eta) = \sum_{i=0}^{\infty} b_{n,i}\eta^i \tag{34}$$

The boundary conditions at the wall $F_n(0)=0$ and $G_n'(0)=0$, namely constant temperature and non-permeability to species , are used to calculate the coefficients $a_{n,i}$ and $b_{n,i}$ by the recursive relations represented by eq. 35 and eq. 36, respectively.

$$a_{n,0} = 0, a_{n,1} = 1, a_{n,2} = 0, a_{n,3} = 0, a_{n,i} = \frac{\lambda_n^{\,2}\,\mathrm{Pr}\left(a_{n,i-4} - 2a_{n,i-3}\right)}{i(i-1)}, i \geq 4 \tag{35}$$

$$b_{n,0} = 1, b_{n,1} = 0, b_{n,2} = 0, b_{n,3} = -\lambda_n^{\,2}/3,$$

$$b_{n,i} = \frac{\lambda_n^{\,2} Sc\left(b_{n,i-4} - 2b_{n,i-3}\right)}{i(i-1)}, i \geq 4 \tag{36}$$

The coefficients A_n and B_n are determined by using a Sturm–Liouville orthogonality condition at the inlet and the boundary conditions at the interface. The solution method follows the procedure presented in (28) although the inlet temperature value in this case is different from the constant value at the wall. Equations 37 and 38 are expressed by multiplying the right-side members of eq. 26 and eq. 27 by the eigenfunctions F_m and G_m, respectively, in the specified order and integrating with respect to η. This is expressed as follows:

$$\lambda_n^2 \,\mathrm{Pr}\int_0^1 \left(2\eta-\eta^2\right) F_m F_n d\eta = -\int_0^1 F_m F_n''\, d\eta = F_m(0)F_n'(0) - F_m(1)F_n'(1) + \int_0^1 F_m' F_n'\, d\eta \qquad (37)$$

$$\lambda_n^2 Sc\int_0^1 \left(2\eta-\eta^2\right) G_m G_n d\eta = -\int_0^1 G_m G_n''\, d\eta = G_m(0)G_n'(0) - G_m(1)G_n'(1) + \int_0^1 G_m' G_n'\, d\eta \qquad (38)$$

The corresponding equations (obtained by proceeding in the same way for eigenvalues and eigenfunctions with index m) are subtracted and the boundary conditions expressed in eq. 30 and eq. 31 are used to yield eq. 39 and eq. 40 as follows:

$$\mathrm{Pr}\left(\lambda_n^2 - \lambda_m^2\right)\int_0^1 \left(2\eta-\eta^2\right) F_n F_m d\eta = F_n(1)F_m'(1) - F_m(1)F_n'(1) \qquad (39)$$

$$Sc\left(\lambda_n^2 - \lambda_m^2\right)\int_0^1 \left(2\eta-\eta^2\right) G_n G_m d\eta = G_n(1)G_m'(1) - G_m(1)G_n'(1) \qquad (40)$$

The coupling between the previous two conditions is established by using eq. 30 and eq. 31 as follows:

$$F_n(1)F_m'(1) - F_m(1)F_n'(1) = -\frac{\Lambda}{Le}\frac{B_n B_m}{A_n A_m}\left[G_n(1)G_m'(1) - G_m(1)G_n'(1)\right] \qquad (41)$$

Equation 41 enables the combination of eq. 39 and eq. 40 as follows:

$$Sc\left(\lambda_n^{\,2}-\lambda_m^{\,2}\right)\int_0^1\left(2\eta-\eta^2\right)\left(\mathrm{Pr}\,LeA_nA_mF_nF_m+Sc\Lambda B_nB_mG_nG_m\right)d\eta=0 \tag{42}$$

This directly implies,

$$\int_0^1\left(2\eta-\eta^2\right)\left(\mathrm{Pr}\,LeA_nA_mF_nF_m+Sc\Lambda B_nB_mG_nG_m\right)d\eta\begin{cases}=0, n\neq m\\ \neq 0, n=m\end{cases} \tag{43}$$

The boundary conditions of constant temperature and mass fraction are used over the entire film thickness at the inlet of the calculation domain as follows:

$$\sum_{n=1}^{\infty}A_nF_n(\eta)=\theta_{in} \tag{44}$$

$$\sum_{n=1}^{\infty}B_nG_n(\eta)=1 \tag{45}$$

The summation of the integrals is simplified as follows:

$$\sum_{n=1}^{\infty}\int_0^1\left(2\eta-\eta^2\right)(\mathrm{Pr}\,LeA_nA_mF_nF_m+Sc\Lambda B_nB_mG_nG_m)d\eta=\int_0^1\left(2\eta-\eta^2\right)(\mathrm{Pr}\,Le\theta_{in}A_mF_m+Sc\Lambda B_mG_m)d\eta \tag{46}$$

According to eq. 43, the first relation between A_n and B_n can be obtained in eq. 44, while the second relation is expressed by either eq. 30 or eq. 31.

$$\int_0^1\left(2\eta-\eta^2\right)(\mathrm{Pr}\,LeA_n^{\,2}F_n^{\,2}+Sc\Lambda B_n^{\,2}G_n^{\,2})d\eta=\int_0^1\left(2\eta-\eta^2\right)(\mathrm{Pr}\,Le\theta_{in}A_nF_n+Sc\Lambda B_nG_n)d\eta \tag{47}$$

Finally, A_n and B_n are solved for as follows:

$$A_n = B_n \frac{G_n(1)}{F_n(1)} \tag{48}$$

$$B_n = \frac{\int_0^1 \left(2\eta - \eta^2\right)\left(\Pr Le\theta_{in} \frac{G_n(1)}{F_n(1)} F_n(\eta) + Sc\Lambda G_n(\eta)\right) d\eta}{\int_0^1 \left(2\eta - \eta^2\right)\left(\Pr Le \frac{{G_n}^2(1)}{{F_n}^2(1)} {F_n}^2(\eta) + Sc\Lambda {G_n}^2(\eta)\right) d\eta} \tag{49}$$

As a result, temperature and mass fraction fields are expressed in eq.s 50 and 51.

$$T(\varepsilon,\eta) = T_W + \left(T_e - T_W\right)\sum_{n=1}^{\infty}\left[A_n \sum_{i=0}^{\infty}\left(a_{n,i}\eta^i\right) e^{-\lambda_n^2 d^*\left(\frac{4WR}{3\mathrm{Re}}\right)^{4/3}\int_0^{\varepsilon}\sin^{1/3}\pi\varepsilon d\varepsilon}\right] \tag{50}$$

$$\omega(\varepsilon,\eta) = \omega_e + \left(\omega_{in} - \omega_e\right)\sum_{n=1}^{\infty}\left[B_n \sum_{i=0}^{\infty}\left(b_{n,i}\eta^i\right) e^{-\lambda_n^2 d^*\left(\frac{4WR}{3\mathrm{Re}}\right)^{4/3}\int_0^{\varepsilon}\sin^{1/3}\pi\varepsilon d\varepsilon}\right] \tag{51}$$

4. Results

The following analysis is performed for a set of representative operative conditions of the absorber in a cooling system (Table 1) and LiBr-H_2O solution properties (49) are calculated for the values of temperature, pressure, and mass fraction. Subsequently, the main influential dimensionless parameters are calculated and listed in Table 2.

Table 1. Operative conditions

T_{in} (°C)	T_W (°C)	ω_{in} (%)	P (kPa)	r (m)	β Ref. (39)
40	32	60	1.0	0.0090	32 °

Table 2. Operative dimensionless parameters

Le	Λ	Sc	Pr	d*	Re	Re_0
110.8	5.515	2567	23.17	568.4	42.95	95.00

Figures 3(a) and 3(b) compare temperature and mass fraction fields, respectively, as obtained with the first 9 eigenvalues/eigenfunctions of the present analytical solution (Table 3) to the corresponding numerical solutions of energy and species transport equations. Both fields indicate good agreement. However, the temperature distribution specifically appears as a rough approximation at the entrance region in proximity to the wall ($\varepsilon \sim 0$), where the highest deviations with respect to the numerical results are observed.

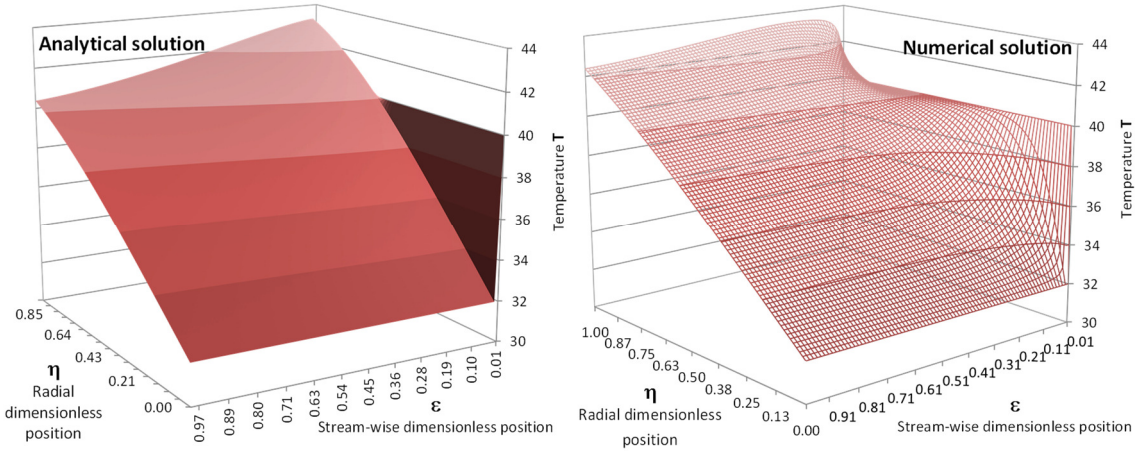

(a)

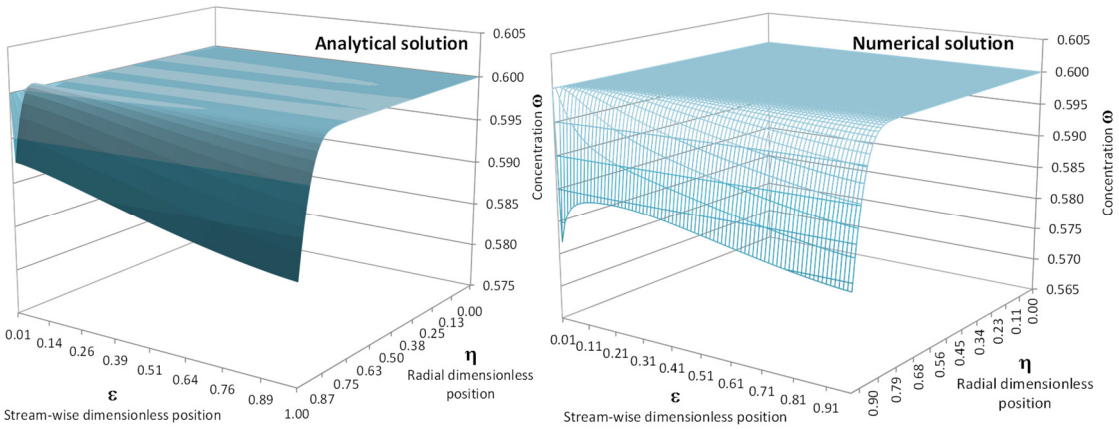

(b)

Figure 3. Film temperature (a) and mass fraction (b) fields in the operative conditions listed in Table 1

It is noteworthy to highlight the agreement between the two solution methods at the film interface, where two different

equilibrium relations are employed. Equation 23 is used for writing the analytical solution, whereas, the thermo-physical properties from (49) are used when numerically solving eq.s 10 and 11. A larger number of eigenvalues and terms representing the eigenfunctions F_n and G_n are considered, and it is possible to model the entrance region with increased accuracy. However, in the case of a subcooled or superheated inlet solution, given the very small values of the coefficient B_n for eigenvalues higher than 9 (Table 3), which goes beyond the number of significant figures available on the calculation platform, this creates instability of the analytical solution away from the wall and specifically close to the film interface (η=1).

The temperature field close to the tube surface obtained with the first 14 eigenvalues (Table 4) is compared to the corresponding numerical solution in Figure 4. It is observed that this enables the analytical solution to model the gradual transition of the temperature distribution at the entrance region in proximity to the wall. Hence, the heat transfer at the tube surface is estimated by considering 14 eigenvalues as listed in Table 3.

Table 3. Eigenvalues and eigenfunction coefficients

n	λ_n	A_n	B_n
1	0.0418	0.129	1.34
2	0.116	0.133	-0.551
3	0.189	0.154	0.369
4	0.259	0.176	-0.275
5	0.326	0.168	0.196
6	0.392	0.113	-0.121
7	0.462	0.0536	0.0610
8	0.533	0.0194	-0.0243
9	0.607	0.00328	0.00440
10	2.26	1.28	-9.00E-45
11	3.06	-0.368	-1.00E-70
12	3.91	1.26	-3.00E-45
13	4.72	-0.504	-1.00E-107
14	5.53	1.27	-8.00E-121

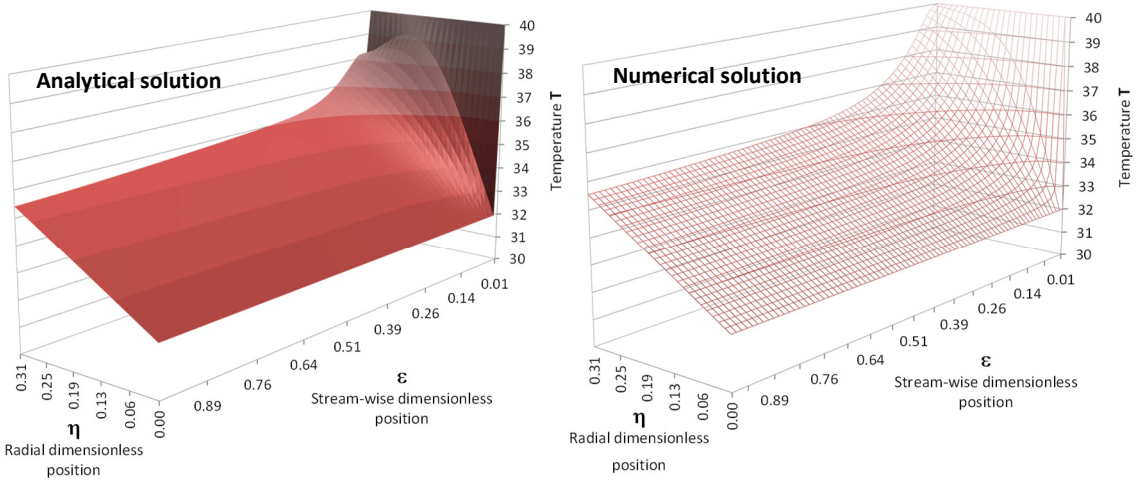

Figure 4. Film temperature field in proximity to the tube wall

5. Heat and mass transfer coefficients

It is assumed that the reduction of the surface in the vapour absorption is represented by the values of *WR*, and thus the local heat and mass transfer coefficient (*htc* and *mtc*) are defined by eq. 52 and eq. 53, respectively, and by eq. 54 and eq. 55, respectively, with respect to the dimensionless parameters (i.e., Nusselt and Sherwood Numbers).

$$htc = WR\frac{k\left.\frac{\partial T}{\partial y}\right|_W}{T_{av} - T_W} \tag{52}$$

$$mtc = -WR\frac{D}{\omega_{if}}\frac{\left.\frac{\partial \omega}{\partial y}\right|_{if}}{\omega_W - \omega_{if}} \tag{53}$$

$$Nu(\varepsilon) = \left(\frac{4}{3}\frac{WR^4 \sin \pi\varepsilon}{\mathrm{Re}}\right)^{1/3} \frac{\sum_{n=1}^{\infty}\left[\frac{G_n(1)}{F_n(1)} B_n a_{n,1} e^{-\lambda_n^2 d^*\left(\frac{4WR}{3\mathrm{Re}}\right)^{4/3}\int_0^{\varepsilon}\sin^{1/3}\pi\varepsilon d\varepsilon}\right]}{\sum_{n=1}^{\infty}\left[\frac{G_n(1)}{F_n(1)} B_n \sum_{i=0}^{\infty}\left(\frac{a_{n,i}}{i+1}\right) e^{-\lambda_n^2 d^*\left(\frac{4WR}{3\mathrm{Re}}\right)^{4/3}\int_0^{\varepsilon}\sin^{1/3}\pi\varepsilon d\varepsilon}\right]} \tag{54}$$

$$Sh(\varepsilon)=$$

$$\frac{\left(\frac{4}{3}\frac{WR^4\sin\pi\varepsilon}{\mathrm{Re}}\right)^{1/3}}{\left\{\omega_e+(\omega_{in}-\omega_e)\sum_{n=1}^{\infty}\left[B_n\sum_{i=0}^{\infty}(b_{n,i})e^{-\lambda_n^2 d^*\left(\frac{4WR}{3\mathrm{Re}}\right)^{4/3}\int_0^{\varepsilon}\sin^{1/3}\pi\varepsilon d\varepsilon}\right]\right\}}\frac{\sum_{n=1}^{\infty}\left[B_n\sum_{i=1}^{\infty}(ib_{n,i})e^{-\lambda_n^2 d^*\left(\frac{4WR}{3\mathrm{Re}}\right)^{4/3}\int_0^{\varepsilon}\sin^{1/3}\pi\varepsilon d\varepsilon}\right]}{\sum_{n=1}^{\infty}\left[B_n\sum_{i=1}^{\infty}(b_{n,i})e^{-\lambda_n^2 d^*\left(\frac{4WR}{3\mathrm{Re}}\right)^{4/3}\int_0^{\varepsilon}\sin^{1/3}\pi\varepsilon d\varepsilon}\right]} \quad (55)$$

The denominators of these last two expressions represent the driving potentials for heat transfer and that for mass transfer, respectively; in the analytical formulation of the Nusselt number, corresponding to the temperature difference between the bulk value of the liquid film and the solid wall; in the expression of the Sherwood number, the difference between the mass fraction at the interface and at the tube wall. On the right-side of the expressions, the numerators include terms corresponding to the temperature gradient at the tube wall and the mass fraction gradient at the film interface. Hence, the factors on the extreme left-side embody the products of the active extension of the film interface and the inverse of the variation of the film thickness while normalised with respect to the characteristic length L_C.

First, the inferences of the main parameters are locally examined for the reference conditions of the absorber as listed in Table 1, and the results obtained are compared while considering the effect of partial wetting (continuous lines) with the solution obtained when the effect is ignored (dashed lines). Figure 5 describes the local Nusselt number distribution along the tube surface. The large temperature difference between the tube wall and the impinging solution at the entrance region is responsible for a local peak in the Nusselt number. Additionally, a local maximum that is positioned in proximity of the vertical part of the tube (ε~0.5) is ascribed to the minimum film thickness. Conversely, in the second half of the tube, the

thickening of the film is associated to a decreasing trend of the local Nusselt number. It is also stated that higher flowrates extend the region affected by the development of the thermal boundary-layer and are responsible for moving the first local minimum of the heat transfer coefficient to higher stream-wise positions. This trend matches the trend presented in extant studies when the governing equations of horizontal tube falling film absorption are numerically solved (16), and the highest deviation occurs in proximity of the inlet of the calculation domain in which the temperature gradient is steeper due to the boundary condition of constant tube wall temperature. The discrepancy between the analytical solution and the numerical solution of the governing equations (eqs. 10-11) increases when the solution flowrate increases. The remaining deviations are related to the assumption of a linear equilibrium-relationship at the interface.

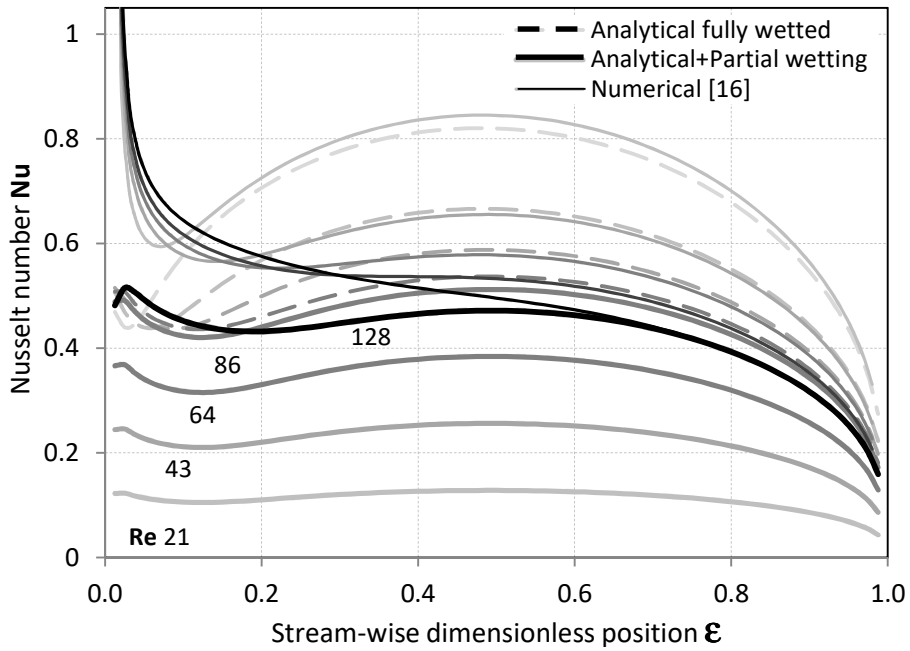

Figure 5. Local Nusselt number corresponding to the first 14 eigenfuntions for different solution mass flowrates at the reference conditions of a refrigerating machine

Figure 5 shows a comparison of continuous and dashed lines of corresponding colours and highlights that low Reynolds

conditions are associated with a globally higher heat transfer rate if partial wetting is overlooked while a gradual reduction in the heat transfer coefficient that is mainly related to the decreasing wetting ability of the solution is experimentally observed (7–11).

In figure 6, the mass transfer at the film interface is locally considered in terms of Sherwood number and indicates a maximum value that grows and moves forward when the solution flowrate increases in the partial wetting region (as shown by the continuous lines).

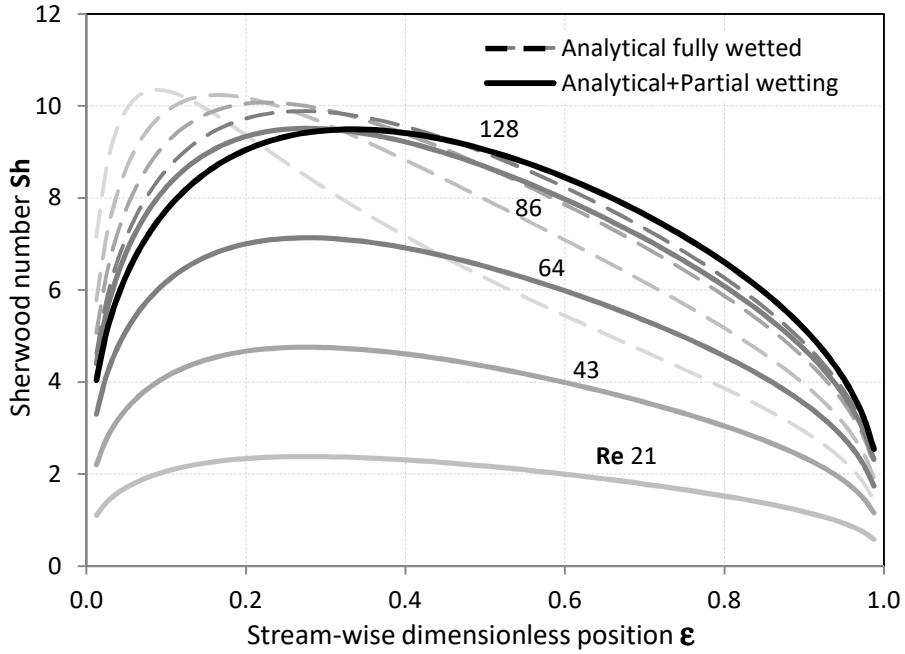

Figure 6. Local Sherwood number for different solution mass flowrates at the reference conditions of a refrigerating machine

Table 4 displays the eigenvalues and their respective eigenfunctions coefficients for two different temperatures at the tube wall of the absorber. A change in this parameter causes the eigenvalues from the characteristic equation (eq. 32) and eigenfunctions coefficients to assume different values.

Table 4. Eigenvalues and coefficients with wall temperatures corresponding to 28℃ and 36℃

n		λ_n	A_n	B_n		λ_n	A_n	B_n
1		0.0424	0.103	1.35		0.0409	0.171	1.33
2		0.118	0.112	-0.571		0.114	0.162	-0.517
3		0.191	0.144	0.407		0.186	0.156	0.310
4		0.262	0.199	-0.337		0.256	0.137	-0.196
5		0.327	0.231	0.271		0.325	0.0971	0.113
6		0.391	0.168	-0.185		0.395	0.0477	-0.0497
7	T_W 28℃	0.459	0.0819	0.105	T_W 36℃	0.465	0.00537	0.00543
8		0.531	0.0368	-0.0554		0.537	-0.0205	0.0207
9		0.605	0.0177	0.0296		0.609	-0.0340	-0.0345
10		2.23	1.40	-1.E-43		2.30	0.991	-3.E-46
11		3.03	-0.282	-9.E-70		3.10	-0.419	-1.E-71
12		3.83	1.24	-4.E-89		3.90	1.06	-8.E-91
13		4.63	-0.316	-4.E-106		4.70	-0.597	-4.E-107
14		5.45	1.20	-2.E-119		5.51332	1.18	-2.E-120

As a rule, a lower wall temperature enhances heat and mass transfer both locally (Figures 7–8) and globally.

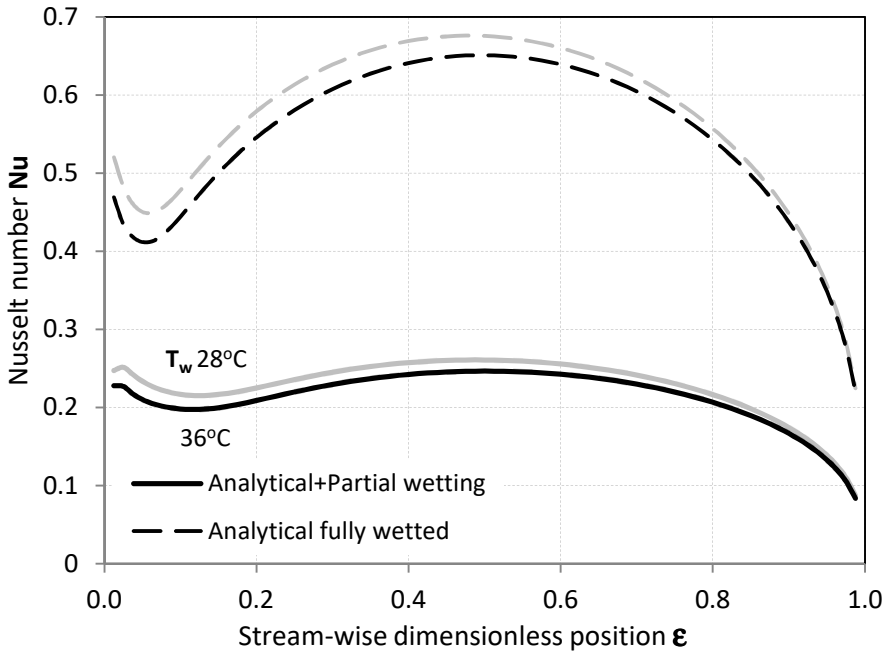

Figure 7. Local Nusselt number for different T_W at reference conditions of a refrigerating machine

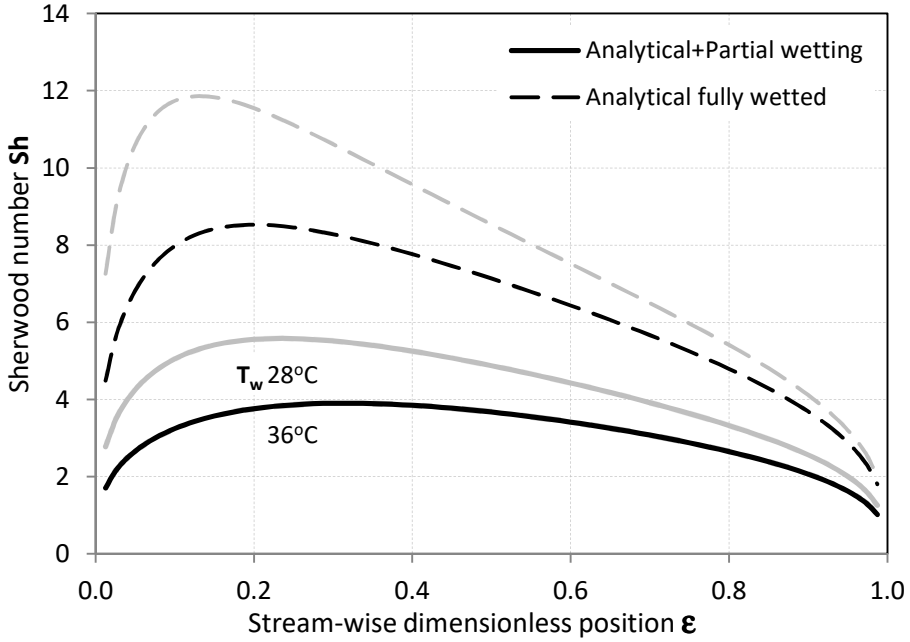

Figure 8. Local Sherwood number for different tube T_W at reference conditions of a refrigerating machine

The wall temperature affects the Sherwood number through the interfacial temperature and consequently changes the interface mass fraction due to the equilibrium hypothesis. Therefore, a lower heat sink temperature can significantly enhance the system capacity by increasing the amount of refrigerant that steadily circulates within the system for a specific solution flowrate.

A local analysis further suggests (50) that a lower tube radius globally increases heat and mass transfer coefficients although it reduces the heat flux per unit length due to a lower heat transfer surface. Accordingly, the best selection of the tube size results from a compromise between the conflicting effects.

The local values of *htc* and *mtc* around the tube are averaged to perform a global analysis for the absorber tube in a wide range of flowrates. Figures 9 and 10 show that heat and mass transfer coefficients are maximised at a certain solution mass flowrate based on the extension of the region affected by partial wetting.

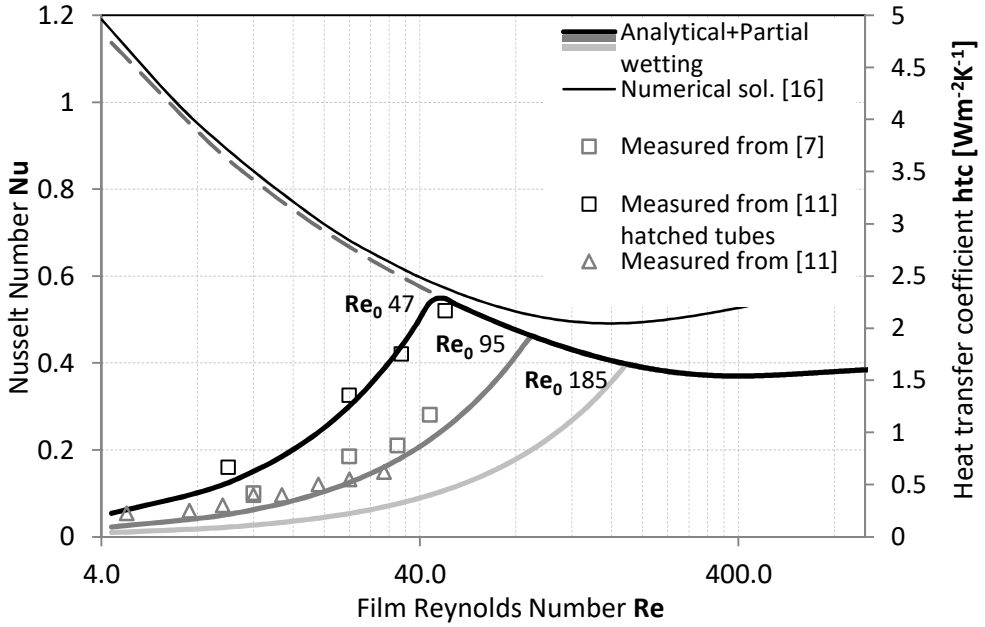

737

738 **Figure 9. Global Nusselt Number for different wetting behaviours at the reference conditions of a**
739 **refrigerating machine**

740

741 The wettability of LiBr-H_2O solution (eq. 5) is increased if
742 tensioactive substances are added to the mixture to decrease the
743 surface tension σ at the vapour-liquid interface or if the solid
744 surface is properly treated (11) to lower the contact angle β at
745 the solid liquid interface. This stabilises thinner uniform
746 films (eq. 4) and moves the occurrence of the film breaking at a
747 lower Reynolds number Re_0. In contrast, if the affinity between
748 the tube surface and the solution worsens, dry patches also
749 appear at higher Reynolds numbers due to impurities or surface
750 roughness. These two cases are qualitatively represented by the
751 lines labelled as Re_0 *47* (the simulations are performed by
752 considering $\beta'=\beta/2$) and Re_0 *185* ($\beta''=2\beta$) in figures 9 and 10,
753 respectively, while Re_0 95 represents the case of smooth tubes
754 at reference conditions for a Lithium-Bromide refrigeration
755 machine (Table 1). The dashed line and thin continuous line
756 represent the analytical solution and the numerical results
757 obtained, respectively, when partial wetting (*WR*=1) over the
758 entire range of operative conditions is neglected.

759 Generally, it is highlighted that both heat and mass transfer
760 are critically improved by improving solution wettability. In
761 the case in which a partial wetting model is not included, the
762 simulated heat transfer coefficients follow an increasing trend
763 to decrease the solution mass flowrates. However, this behaviour
764 is in disagreement with all the experimental results indicated in
765 previous studies (5–11). This indicates the necessity to consider
766 partial wetting phenomena in the standard operative range of
767 absorbers operating in real plants.
768

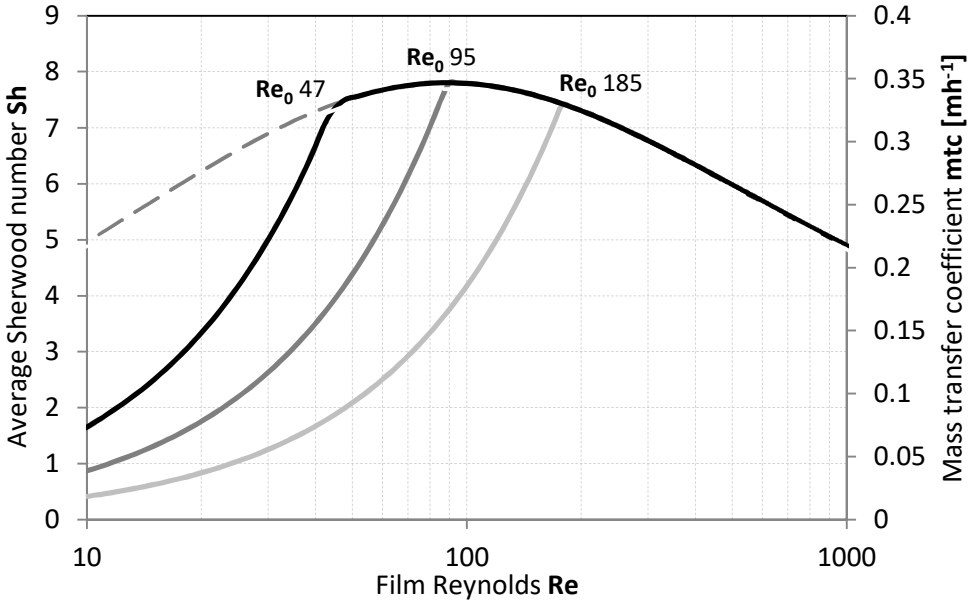

769
770 **Figure 10. Global Sherwood number for different wetting behaviours at reference conditions of a**
771 **refrigerating machine**
772

773 **7. Conclusions**

774 The presented model for laminar falling film absorption over a
775 horizontal cooled tube considers the cylindrical shape of the
776 tube, the effect of partial wetting, thickness variation of the
777 film flowing around the tube, and arbitrarily selected inlet
778 conditions. A simplified linear model for partial wetting is
779 included to extend the validity of the obtained expressions when
780 complete wetting is not considered as a valid assumption. The
781 model provides detailed information to locally and globally

characterise heat and mass transfer of falling film absorbers. The effects related to partial wetting and the main geometrical and operative parameters are investigated to extract general guidelines to optimise the aforementioned devices.

Low Reynolds conditions are associated with a globally higher heat transfer rate when partial wetting is overlooked. Conversely, a gradual reduction in the heat transfer coefficient that was mainly related to the decreasing wetting ability of the solution was experimentally observed in previous studies. In general, the results highlight that both heat and mass transfer are critically improved by improving solution wettability.

The study indicates the possibility of an optimal tube radius from a compromise between lower heat flux per unit length and higher heat and mass transfer coefficients.

Average heat and mass transfer coefficients around the tube are analysed in a wide range of flowrates and show that heat and mass transfer coefficients are maximised at a certain solution mass flowrate based on the extension of the region affected by partial wetting.

Given the observed qualitative and quantitative agreements, it is possible to employ the model as a computationally light and accurate module in component and system simulations to design and control actual systems.

References

(1) A. Lubis, J. Jeong, K. Saito, N. Giannetti, H. Yabase, M.I. Alhamid, Nasruddin, (2016), Solar-assisted single-double-effect absorption chiller for use in Asian tropical climates, Renewable Energy, Vol. 99, pp. 825–835.

(2) N. Giannetti, A. Rocchetti, K. Saito, (2016), Thermodynamic optimization of three-thermal irreversible systems, International Journal of Heat and Technology, Vol. 34, pp. S83–S90.

(3) N. Giannetti, A. Rocchetti, A. Lubis, K. Saito, S. Yamaguchi, (2016), Entropy parameters for falling film absorber optimization, Applied Thermal Engineering, Vol. 93, pp. 750–762.

(4) N. Giannetti, A. Rocchetti, K. Saito, S. Yamaguchi, (2015), Irreversibility analysis of falling film absorption over a cooled horizontal tube, International Journal of Heat and Mass Transfer, Vol. 88, pp. 755–765.

(5) K. Saito, N. Inoue, Y. Nakagawa, Y. Fukusumi, H. Yamada, T. Irie, (2015), Experimental and numerical performance evaluation of double-lift absorption heat transformer, Science and Technology for the Built Environment, Vol. 21, pp. 312–322.

(6) A. Lubis, N. Giannetti, S. Yamaguchi, K. Saito, N. Inoue, (2017), Experimental performance of a double-lift absorption heat transformer for manufacturing-process steam generation, Energy Conversion and Management, Vol. 148, pp. 267-278.

(7) L. Hoffmann, I. Greiter, A. Wagner, V. Weiss, G. Alefeld, (1996), Experimental investigation of heat transfer in a horizontal tube falling film absorber with aqueous solutions of LiBr with and without surfactants, International Journal of Refrigeration, Vol. 19 (5), pp. 331–341.

(8) I. Kyung, K.E. Herold, Y.T. Kang, (2007), Experimental verification of H_2O/LiBr absorber bundle performance with smooth horizontal tubes, International Journal of Refrigeration, Vol. 30 (4), pp. 582–590.

(9) V.M. Soto Francés, J.M. Pinazo Ojer, (2003), Validation of a model for the absorption process of H_2O(vap) by a LiBr(aq) in a horizontal tube bundle using a multi-factorial analysis, International Journal of Heat and Mass Transfer, Vol. 46, pp. 3299–3312.

(10) S.M. Deng, W.B. Ma, (1999), Experimental studies on the characteristics of an absorber using LiBr/H_2O solution as working fluid, International Journal of Refrigeration, Vol. 22, pp. 293–301.

(11) C.W. Park, S.S. Kim, H.C. Cho, Y.T. Kang, (2003), Experimental correlation of falling film absorption heat transfer on micro-scale hatched tubes, International Journal of Refrigeration, Vol. 26 (7), pp.758–763.

(12) S.S. Kim, C.W. Park, H.C. Cho, Y.T. Kang, (2003), The effect of micro-scale surface treatment on heat and mass transfer performance for a falling film H2O/LiBr absorber, International Journal of Refrigeration, Vol. 26 (5), pp. 575–585.

(13) M. Mittermaier, P. Schulze, F. Ziegler, (2014), A numerical model for combined heat and mass transfer in a laminar liquid falling film with simplified hydrodynamics, International Journal of Heat and Mass Transfer, Vol. 70, pp. 990–1002.

(14) J.W. Andberg, G.C. Vliet, (1987), A simplified model for absorption of vapors into liquid films flowing over cooled horizontal tubes, ASHRAE Trans, Vol. 93, pp. 2454–66.

(15) V.D. Papaefthimiou, I.P. Koronaki, D.C. Karampinos, E.D. Rogdakis, (2012), A novel approach for modelling LiBr–H_2O falling film absorption on cooled horizontal bundle of tubes, International Journal of Refrigeration, Vol. 35 (4), pp. 1115–1122.

(16) F. Babadi, B. Farhanieh, (2005), Characteristics of heat and mass transfer in vapor absorption of falling film flow on a horizontal tube, International Communications in Heat and Mass Transfer, Vol. 32 (9), pp.1253–1265.

(17) G. Kocamustafaogullari, I.Y. Chen, (1988), Falling film heat transfer analysis on a bank of horizontal tube evaporator, AIChE Journal, Vol. 34 (9), pp. 1539–1549.

(18) L. Harikrishnan, S. Tiwari, M.P. Maiya, (2011), Numerical study of heat and mass transfer characteristics on a falling film horizontal tubular absorber for R-134a-DMAC, International Journal of Thermal Sciences, Vol. 50 (2), pp. 149–159.

(19) V. Subramaniam, S. Garimella, (2014), Numerical study of heat and mass transfer in lithium bromide-water falling films and droplet, International Journal of Refrigeration, Vol. 40, 211–226.

(20) V. Subramaniam, S.rinivas Garimella, (2009), From measurements of hydrodynamics to computation of species transport in falling films, International Journal of Refrigeration, Vol. 32 (4), pp. 607–626.

(21) Q. Qiu, C. Meng, S. Quan, W. Wang, (2017), 3-D simulation of flow behaviour and film distribution outside a horizontal tube, International Journal of Heat and Mass Transfer, Vol. 107, pp. 1028-1034.

(22) S.M. Hosseinnia, M. Naghashzadegan, R. Kouhikamali, (2016), CFD simulation of adiabatic water vapor absorption in large drops of water–LiBr solution, Applied Thermal Engineering, Vol. 102, pp. 17-29.

(23) Y. Zhou, Z. Cai, Z. Ning, M. Bi, (2017), Numerical simulation of double-phase coupled heat transfer process of horizontal-tube falling film evaporation, Applied Thermal Engineering, Vol. 118, pp. 33-40.

(24) S.M. Hosseinnia, M. Naghashzadegan, R. Kouhikamali, (2017), CFD simulation of water vapor absorption in laminar falling film solution of water-LiBr — Drop and jet modes, Applied Thermal Engineering, Vol. 115, pp. 860-873.

(25) G. Ji, J. Wu, Y. Chen, G. Ji, (2017), Asymmetric distribution of falling film solution flowing on hydrophilic horizontal round tube, International Journal of Refrigeration, Vol. 78, pp. 83-92.

881 (26) N.I. Grigor'eva, V.E. Nakoryakov, (1977), Exact solution of a combined Heat- and
882 Mass- transfer problem during film absorption, Inzhernerno-Fizicheskii Zhurnal, Vol. 33 (5), pp.
883 893–898.
884 (27) S. K. Choudhury, A. Nishiguchi, D. Hisajima, T. Fukushima, T. ohuchi, S. Sakaguchi,
885 (1993), Absorption of vapors into liquid films flowing over cooled horizontal tubes, ASHRAE
886 Transaction, Vol. 99 (2), pp. 81–89.
887 (28) G. Grossman, (1983), Simultaneous heat and mass transfer in film absorption under
888 laminar flow, International Journal of Heat and Mass Transfer, Vol. 26 (3), pp. 357–371.
889 (29) T. Meyer, F. Ziegler, (2014), Analytical solution for combined heat and mass transfer in
890 laminar falling film absorption using first type boundary conditions at the interface,
891 International Journal of Heat and Mass Transfer, Vol. 73, pp. 141–151.
892 (30) M.J. Kirby, H. Perez-Blanco, (1994), A Design Model for Horizontal Tube
893 Water/Lithium Bromide Absorbers, Heat pump and refrigeration systems design, analysis, and
894 applications, ASME-PUBLICATIONS- AES, Vol. 32, pp. 1-10.
895 (31) J. Wu, Z. Yi, Y. Chen, R. Cao, C. Dong, S. Yuan, (2015), Enhanced heat and mass
896 transfer in alternating structure of tubes and longitudinal trough mesh packing in lithium
897 bromide solution absorber, International Journal of Refrigeration, Vol. 53, pp. 34-41.
898 (32) S. Jeong, S. Garimella, (2002), Falling-film and droplet mode heat and mass transfer in
899 a horizontal tube LiBr/water absorber, International Journal of Heat and Mass Transfer, Vol. 45
900 (7), pp. 1445–1458.
901 (33) V. M. Soto Francés, J. M. Pinazo Ojer, Experimental study about heat and mass transfer
902 during absorption of water by an aqueous lithium bromide solution, International Proceedings of
903 the ASME-ZSITS International Thermal Science Seminar, Bled (Slovenia), 11–14 June, (2000),
904 pp. 535–542.
905 (34) N. Giannetti, A. Rocchetti, S. Yamaguchi, K. Saito, (2017), Analytical solution of film
906 mass-transfer on a partially wetted absorber tube, International Journal of Thermal Sciences,
907 Vol. 118, pp. 176-186.
908 (35) Y. Chen, R. Cao, J. Wu, Z. Yi, G. Ji, (2016), Alternate heat and mass transfer
909 absorption performances on staggered tube bundle with M–W corrugated mesh guider inserts,
910 International Journal of Refrigeration, Vol. 66, pp. 10-20.
911 (36) R.H. Wassenaar, (1996), Measured and predicted effect of flowrate and tube spacing on
912 horizontal tube absorber performance, International Journal of Refrigeration, Vol. 19 (5), pp.
913 347–355.

(37) Y. Lazcano-Véliz, J. Siqueiros, D. Juárez-Romero, L.I. Morales, J. Torres-Merino, (2014), Analysis of effective wetting area of a horizontal generator for an absorption heat transformer, Applied Thermal Engineering, Vol. 62 (2), pp. 845–849.

(38) K.S. Lee, B. Köroğlu, C. Park, (2012), Experimental investigation of capillary-assisted solution wetting and heat transfer using a micro-scale, porous-layer coating on horizontal-tube, falling-film heat exchanger, International Journal of Refrigeration, Vol. 35 (4), pp. 1176–1187.

(39) B. Köroğlu, K.S. Lee, C. Park, (2013), Nano/micro-scale surface modifications using copper oxidation for enhancement of surface wetting and falling-film heat transfer, International Journal of Heat and Mass Transfer, Vol. 62, pp. 794–804.

(40) D. M. Maron, G. Ingel, N. Brauner, (1982), Wettability and break-up of thin films on inclined surfaces with continuous and intermittent feed, Desalination, Vol. 42, pp. 87–96.

(41) J. Tang, Z. Lu, B. Yu-Chi, S. Lin, (1991), Minimum Wetting Rate of Film Flow on Solid Surface, Proceedings of the 18th International Congress of Refrigeration, Vol. 2, pp. 519–523, Montreal.

(42) J. Mikielewicz, J. R. Moszynski, (1976), Minimum thickness of a liquid film flowing vertically down a solid surface, lnternational Journal of Heat and Mass Transfer, Vol. 19, pp. 771–776.

(43) N. Giannetti, S. Yamaguchi, K. Saito, (2016), Wetting behaviour of a liquid film on an internally-cooled desiccant contactor, International Journal of Heat and Mass Transfer, Vol. 101, pp. 958–969.

(44) C.S. Yih, (1963), Stability of liquid flow down an inclined plane, Phyics of Fluids, Vol. 6, pp. 321-334.

(45) D.E. Hartley, W. Murgatroyd, (1964), Criteria for the break-up of thin liquid layers flowing isothermally over solid surfaces, International Journal of Heat and Mass Transfer, Vol. 7, pp. 1003-1015.

(46) A.B. Ponter, G.A. Davies, T.K. Ross, P.G. Thornley, (1967), The influence of mass transfer on liquid film breakdown, International Journal of Heat and Mass Transfer, Vol. 10, pp. 349-359.

(47) N. Giannetti, D. Kunita, S. Yamaguchi, K. Saito, (2018), Annular flow stability within small-sized channels, International Journal of Heat and Mass Transfer, Vol. 116, pp. 1153-1162.

(48) G. Grossmann, (1982), Simultaneous heat and mass transfer in absorption/desorption of gases in laminar liquid films, Proc. A.I.Ch.E. Winter and Annual Meeting, Orlando, Florida.

(49) (1990), properties of lithium bromide-water solutions at high temperatures and condensations - Part I. Thermal Conductivity, ASHRAE Trans, Vol. 96.

(50) N. Giannetti, A. Rocchetti, K. Saito, S. Yamaguchi, (2016), Analytical description of falling film absorption, Proceedings of the 8th Asian Conference on Refrigeration and Air Conditioning, May 15th –17th, Taipei, Taiwan. https://www.scopus.com/inward/record.uri?eid=2-s2.0-84988972662&partnerID=40&md5=72097627e4b8617ef7168d45b30fd3c1